Acta Crystallographica Section D
Biological Crystallography
ISSN 0907-4449

Crystallization and preliminary X-ray analysis of human RCC1, the regulator of chromosome condensation

Louis Renault,[a,b]* Nicolas Nassar,[c] Alfred Wittinghofer,[a] Michel Roth[b] and Ingrid R. Vetter[a]

[a]Max-Planck-Institut für molekulare Physiologie, Rheinlanddamm 201, 44139 Dortmund, Germany, [b]Institut de Biologie Structurale Jean-Pierre Ebel, Laboratoire de Cristallographie et de Cristallogenèse des Protéines, 41 Avenue des Martyrs, 38027 Grenoble CEDEX 1, France, and [c]Department of Chemistry, Baker Laboratory and Department of Pharmacology, College of Veterinary Medicine, Cornell University, Ithaca, NY 14853, USA

Correspondence e-mail: ingrid.vetter@mpi-dortmund.mpg.de

Received 24 February 1998
Accepted 1 June 1998

RCC1, the regulator of chromosome condensation, is the guanine nucleotide-exchange factor (GEF) of the GTP-binding protein Ran. Its GEF activity on Ran makes it a key element in nucleo-cytoplasmic transport and cell-cycle regulation. Crystals of human RCC1 suitable for X-ray analysis have been obtained using the seeding technique in hanging drops with sodium citrate as a precipitant. The crystals diffract to 1.7 Å at 100 K and belong to the space group $P1$, with unit-cell parameters a = 49.5, b = 84.3, c = 84.9 Å, α = 113.0, β = 103.9, γ = 103.3°. The Matthews parameter (V_m) and the self-rotation function are consistent with three molecules in the unit cell, which is confirmed by the averaged single isomorphous replacement (SIR) electron-density map.

1. Introduction

Regulator of chromosome condensation (RCC1) was first identified from the temperature-sensitive (ts) mutant hamster-cell line tsBN2, as a protein controlling the initiation of chromosome condensation at the entry of mitosis (Kai *et al.*, 1986). The tsBN2 cells, when shifted to non-permissive temperatures (312.5–313 K) during the S phase of the cell cycle, show premature condensation of the chromatin and die. The mutation responsible for the tsBN2 phenotype is localized in the RCC1 gene, which encodes a nuclear DNA-binding protein with a molecular mass of 45 kDa. Because of this mutation (S256T), the RCC1 protein is degraded in this cell line following a temperature shift (Uchida *et al.*, 1990, Nishitani *et al.*, 1991). These results have led Nishimoto and coworkers to propose RCC1 as an element for detecting unreplicated DNA in the S phase and transducing an inhibitory signal to prevent the activation of mitotic factors.

Subsequently, the analysis of mutants of RCC1 homologues has shown that the protein is involved in a number of control systems for pre-messenger RNA processing (Aebi *et al.*, 1990; Kadowaki *et al.*, 1993), mating (Clark & Sprague, 1989), initiation of mitosis (Matsumoto & Beach, 1991) and chromatin decondensation (Sazer & Nurse, 1994). In parallel, biochemical studies have identified RCC1 as the guanine nucleotide-exchange factor (GEF) of the small nuclear GTP-binding protein Ran (Ras-like nuclear GTP-binding protein; Bischoff & Ponstingl, 1991), which is a major component of nucleo-cytoplasmic transport and cell-cycle regulation. Since most of the phenotypes associated with RCC1 mutants are also dependent on the nucleotide state of Ran (Rush *et al.*, 1996), the major role attributed to RCC1 seems to be in the regulation of the GTPase cycle of Ran.

Ran, like all regulatory GTP-binding proteins, catalyzes the hydrolysis of GTP to GDP. It acts as a molecular switch that couples the GTPase cycle to one or more cellular processes. Guanine nucleotide-exchange factors catalyze guanine nucleotide dissociation and thus promote activation. For Ran, its GEF RCC1 increases the otherwise slow release of GDP by a factor of 10^5 (Klebe *et al.*, 1995) and thus favours the binding of GTP, which is in excess over GDP in the intracellular medium. The GTPase reaction, accelerated by RanGAP (Klebe *et al.*, 1995) by a similar rate (10^5-fold), mediates the transition from GTP-bound state to GDP-bound state. The two regulators of this GTPase cycle, RCC1 and RanGAP, belong to two different cellular compartments of the nucleo-cytoplasmic transport: RCC1 is predominantly a nuclear protein, while RanGAP is predominantly located in the cytosol. It remains to be seen whether such compartmentalization plays a crucial role in directional trafficking of protein and RNA through the nuclear pore complex, where both states of Ran are important.

Since Ran is also an active component of mitotic checkpoint control, two domains may coexist in RCC1 to allow the protein to process the different signalling pathways (Seki *et al.*, 1996): one required for taking upstream signals about the conformational change of the chromatin and the other for transferring them downstream through the Ran biological switch.

Among different species, RCC1 is seen to exhibit a variation in its length, ranging from 421 amino acids in human to 547 amino acids in drosophila. However, all RCC1 homologues

© 1999 International Union of Crystallography
Printed in Great Britain – all rights reserved

have seven sequence repeats of about 50–70 amino acids (RCC1 repeats) in common, often preceded by a short N-terminal basic region. This basic N-terminal region was shown to be necessary for DNA binding and important for efficient nuclear import (Seki *et al.*, 1996). Nevertheless, only the repeated domains are essential for coupling mitosis with DNA replication (Seino *et al.*, 1992). The mutual complementation of RCC1 between yeast, *Drosophila*, *Xenopus* and mammalian homologues, in addition to the mapping of the RCC1$^-$ mutants within the RCC1 repeats, suggest that these conserved elements are essential for the function and/or the folding of the protein. Similar RCC1-like motifs have been reported in several non-homologue proteins: P532 which possesses a guanine nucleotide-exchange activity towards Rab and Arf (Rosa *et al.*, 1996), retinitis pigmentosa GTPase regulator (RPGR) which is also a potential guanine nucleotide-exchange factor (Meindl *et al.*, 1996; Roepman *et al.*, 1996) or alpha-tubulin suppressor (ATS1) which is involved in the cellular regulation of microtubule assembly and organization (Kirkpatrick & Solomon, 1994). These repeats are likely to consist mostly of β-strands, as suggested by secondary-structure prediction algorithms.

As a first step towards identifying the nature of the RCC1 repeats and understanding the possible pleiotropic function of the protein, we report here the crystallization and preliminary crystallographic studies of full-length human RCC1.

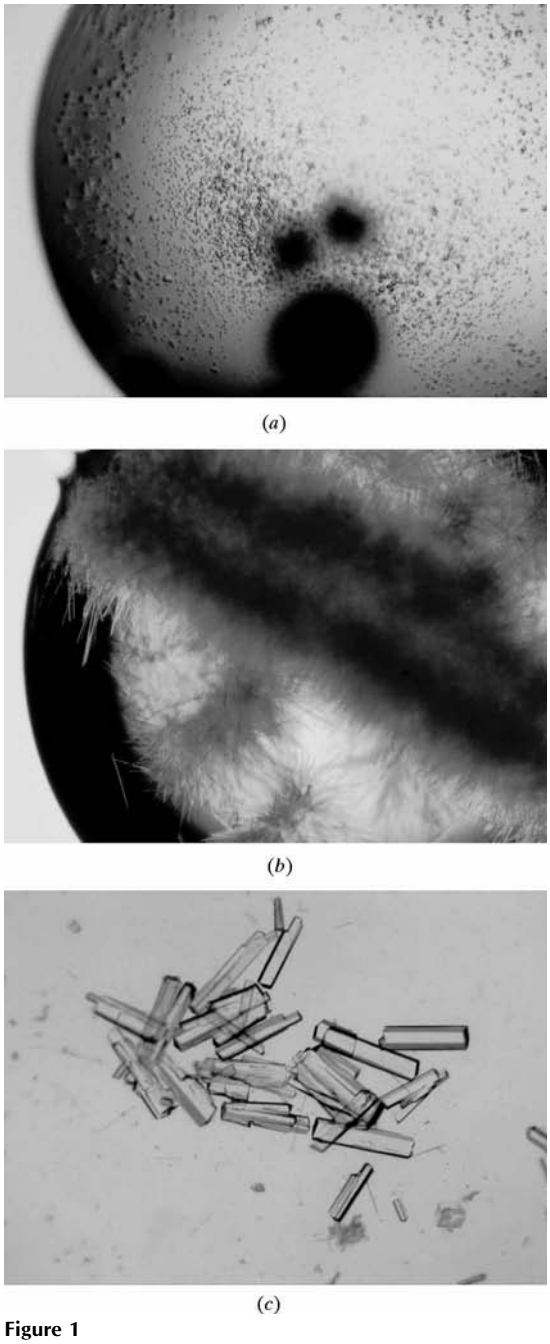

Figure 1
Crystallization of human RCC1. (*a*) Thin crystals obtained without seeding. (*b*) Crystals after the first microseeding in a straight line at reduced concentrations of the precipitant sodium citrate. (*c*) Crystals suitable for X-ray analysis (size approximately 0.15 × 0.05 × 0.05 mm) after a second microseeding procedure with the crystals shown in (*b*).

2. Materials, methods and results

The purification, cloning and expression of this protein in *E. coli* has been described in detail elsewhere (Klebe *et al.*, 1993). The recombinant full-length protein was purified from *E. coli* strain CK600K containing the plasmid ptac, and its activity was checked to be similar to the native protein. The first eight residues are missing as a result of proteolytic processes. The protein is a monomer in solution as shown by gel-filtration studies.

Initial crystals of RCC1 grew at room temperature after 1–2 d from hanging drops (Linbro culture plate) containing equal amounts (1–2 µl) of protein and of reservoir solution (1.25 *M* sodium citrate pH 6.8–7.0 and 2–4 m*M* DTE). These crystals were very thin with a sea-urchin-like appearance (Fig. 1*a*) and were not suitable for X-ray analysis. Attempts to improve the crystal quality by varying precipitant or protein concentration, temperature, pH, buffer, additives or drop volume failed. The crystal quality could, however, be dramatically improved by a microseeding procedure (Ducruix & Giegé, 1992) in which fresh crystals were crushed and inoculated with a fine cat whisker into preequilibrated (overnight) drops (3 µl of 20–15 mg ml^{-1} protein and 3 µl of 1.07 *M* sodium citrate with DTE). The first seeding led to a large number of thin needles (Fig. 1*b*). Upon repeating the microseeding procedure and introducing a smaller number of seeds, crystals suitable for data collection, although small and twinned, were obtained (Fig. 1*c*). In the best case, crystals of size 0.2 × 0.1 × 0.1 mm were obtained after 1–3 months. The largest crystals, mounted in capillaries, diffracted to 2.4 Å on a rotating anode, with a mosaic spread of 0.35°, but were not sufficiently stable in the beam. Crystals which were flash-cooled using standard cryofreezing protocols showed high mosaic spreads (0.9–1.2°) and a diffraction limit of only 2.6 Å. By carefully optimizing the crystal treatment and the cryoprotecting agents as described below, the resolution could be extended to 1.76 Å at 100 K on the rotating anode with a mosaic spread of 0.35°. Unfortunately, crystals of this size could not be reproduced and the frozen crystal diffracting to 1.76 Å was lost. Later, a smaller crystal yielded 1.7 Å data (at 100 K) on a synchrotron.

Most X-ray diffraction data were collected on a three-circle Hi-star Siemens area detector with a Siemens rotating-anode generator and were processed and scaled using *XDS* and *XSCALE* (Kabsch, 1993). One data set to 1.7 Å resolution was collected on a MAR detector at the DORIS storage ring (DESY, Hamburg) on the EMBL X11 beamline at a wavelength of 0.9096 Å and were processed and scaled using *DENZO* and *SCALEPACK* (Otwinowski & Minor, 1993).

The crystals were usually twinned to varying degrees, showing two separate lattices in the diffraction pattern. In some cases, even crystals which looked single on the first glance could be identified as twinned by looking down the long axis of the rod-like crystals using polarized light. Crystals which showed the least amount of secondary lattice were selected and allowed successful autoindexing of the major lattice, ignoring the minor one. Possible Laue symmetries were either triclinic or rhombohedral. Due to the presence of twinning and pseudo-symmetry (see below), the space-group determination was not straightfor-

Table 1
Data-reduction statistics.

Crystal number	1	2	3	1–3 merged
Size (µm)	170 × 150 × 70	170 × 100 × 60	150 × 70 × 50	—
X-ray source	Rotating anode	Rotating anode	X11, DESY	—
Resolution range	41.5–1.76 Å	35.6–2.07 Å	16.5–1.7 Å	—
Unique reflections	85945	52888	104136	114113
Observed reflections	234257	159141	206175	238114
Completeness† (%)	79.9 (56.4)	79.9 (30.8)	87.5 (69.9)	95.6 (71.6)
Redundancy†	2.7 (1.9)	3.0 (1.5)	2.0 (1.5)	—
$\langle I/\sigma \rangle$†	21.33 (4.8)	21.57 (3.88)	11.7 (2.5)	22.22 (3.01)
$R_{\rm sym}$†‡ (%)	4.4 (12.6)	4.3 (13.8)	6.0 (26.5)	8.6 (24.7)

† All data corresponding to the resolution as indicated in the table (last shell in parentheses; 1.9–1.76 Å for crystal 1, 2.11–2.07 Å for crystal 2 and 1.73–1.7 Å for crystal 3 and the merged data set). ‡ $R_{\rm sym} = \sum |I_i(h) - \langle I(h) \rangle| / \sum \langle I(h) \rangle$, where $I_i(h)$ is the intensity measurement for the reflection i and $\langle I(h) \rangle$ is the mean intensity for multiply recorded reflections h.

ward. With respect to the $R_{\rm sym}$ values and the appearance of the diffraction pattern, the crystals seemed to have $R3$ symmetry with unit-cell parameters $a = b = 148.7$, $c = 52.6$ Å, $\alpha = \beta = 90$, $\gamma = 120^\circ$. To verify this, the reflections which were supposed to be related by $R3$ symmetry were systematically analyzed according to Garboczi *et al.* (1994). The intensity differences (weighted by their associated sigmas) between pairs of symmetry-related reflections after scaling in $P1$ are expected to show a sharp distribution around zero if the choice of space group is correct. The presence of a substantial number of intensity differences greater than 4σ would indicate the absence of the corresponding symmetry operator (Garboczi *et al.*, 1994). This analysis clearly eliminated the possibility of a rhombohedral space group so that the true space group could be identified as $P1$ in spite of the pseudosymmetry. The unit-cell parameters were determined to be $a = 49.5$, $b = 84.3$, $c = 84.9$ Å, $\alpha = 113.0$, $\beta = 103.9$, $\gamma = 103.3^\circ$.

Assuming three monomers per unit cell, the Matthews parameter (Matthews, 1968) is 2.10 Å^3 Da^{-1}, corresponding to a solvent content of approximately 41%. This result is consistent with the non-crystallographic peaks observed in the self-rotation function calculated with the *CCP*4 suite (Collaborative Computational Project, Number 4, 1994). In the $\kappa = 120^\circ$ section, a threefold non-crystallographic symmetry is revealed by the presence of a strong peak (60% of the origin peak height) almost along the crystallographic a axis (4° off). The close coincidence of the threefold axis and a crystal axis accounted for the above mentioned pseudosymmetry. Three additional peaks (29% of the origin peak height) are present in the $\kappa = 180^\circ$ section of the rotation function and correspond to three twofold non-crystallographic symmetries. These peaks are perpendicular to the threefold axis and make an angle of 120° with respect to each other. With three protein molecules per unit cell, these twofold peaks can only be explained by the presence of an internal twofold symmetry in each monomer. The existence of internal symmetry in RCC1 is also suggested by the presence of homologous stretches of 60 amino-acid repeats in the primary sequence.

Conditions for flash-cooling were established by stabilizing the crystals overnight in solutions containing slightly higher concentrations of precipitating agent than in the crystal setup before adding cryoprotectant. A first set of cryoprotectants, which did not visibly damage the crystals when added to the mother liquor even after waiting at least a few hours, was selected at room temperature. The optimum concentration of the cryoprotectant was then determined by flash-cooling the crystals and evaluating the mosaic spread and the diffraction limit (Garman & Schneider, 1997). The addition of 15%(*w*/*v*) xylitol and 10%(*v*/*v*) glycerol to the stabilizing solution reproduced the mosaicity observed at room temperature. A slightly smaller mosaicity was observed when transferring the crystals progressively to the final cryoprotectant concentration and then flash-cooling them. With this cryofreezing protocol, the diffraction limit of the crystals increased to 1.76 Å on the in-house rotating anode and the difference in the volume of the unit cell between data sets measured at room temperature and at 100 K was around 5.4%. Ice growing on the loop was removed by washing the loop with liquid nitrogen from time to time. It should be pointed out that the crystals were extremely sensitive to temperature changes or mechanical shock so that only the transport of pre-frozen crystals to the synchrotron prevented loss in diffraction quality.

For the heavy-atom search, three native data sets were merged together to produce a reliable reference data set. Two of these data sets were collected to 1.76 and 2.07 Å resolution (crystal 1 and 2, respectively, in Table 1) on an area detector with a rotating-anode source. The third was collected to a resolution of 1.7 Å with a poor completeness at low resolution on a MAR image-plate detector at the X11 beamline (DESY, Hamburg; crystal 3 in Table 1).

The quality of all data sets was influenced by the existence of varying degrees of twinning as explained above. It was therefore crucial for the heavy-atom search to select the best native data sets and to carefully merge them together to get rid of systematic errors. The merging procedure was optimized by applying anisotropic scaling factors [using *SCALEIT* in the *CCP*4 program suite (Collaborative Computational Project, Number 4, 1994)] to the unique reflections of each data set in order to account for the absorption effects of different crystals.

The presence of citrate, a very good chelator of heavy atoms, at high concentration in the mother liquor required the screening of many heavy-atom compounds before a useful derivative was obtained. After 40 attempts at room temperature and at 100 K, one very good uranyl acetate derivative could be obtained. This derivative was produced by soaking crystals in a saturated solution of uranyl acetate (in 1.25 *M* sodium citrate pH 6.9 for 7.5 h) to overcome the competition of citrate in heavy-atom binding. Although the derivative crystal stayed transparent in this coloured solution, it showed six strong sites in a difference Patterson map. These sites were consistent with the non-crystallographic threefold, as shown in a self-rotation function calculated using the structure-factor differences between the derivative and native crystal data. The derivative crystal diffracted to 2.4 Å resolution with an $R_{\rm iso}$ of 19.9%, which is a factor of two larger than between two native data sets. SIR phases calculated from this derivative showed a figure of merit of 0.39, a phasing power of 1.78 and an $R_{\rm Cullis}$ of 67%. Starting from the experimental SIR phases, density modification and phase extension were carried out in combination with non-crystallographic averaging as described below.

From the heavy-atom positions, an approximate centre of gravity could be defined for each monomer by applying solvent flattening and histogram matching without averaging. By maximizing the correlation coefficients between electron densities defined with respect to these three centres of gravity, the non-crystallographic symmetry operators and the molecular envelopes of one monomer were refined iteratively, using *DEMON* (Vellieux *et al.*, 1995). After this initial refinement, density

modification has been applied with success, combining solvent flattening, histogram matching, non-crystallographic averaging and phase extension to 1.7 Å using the *DM* program from the *CCP*4 program suite (Collaborative Computational Project, Number 4, 1994). The initial electron-density map was already of very high quality. During non-crystallographic averaging, maps using the data to 1.7 Å were always better than the averaged maps at a lower resolution.

An initial model for RCC1 has been obtained (Renault *et al.*, 1998) and is currently being further refined. It should guide us towards a better understanding of how a GEF catalyzes nucleotide exchange on a Ras-related GTP-binding protein and provide an initial idea about the putative bifunctionality of the protein in ensuring DNA binding on one hand and transmission of the signal to Ran on the other.

LR acknowledges the support from IBS/LCCP and the staff at the ESRF synchrotron facility on the beamline CRG D2AM. We also thank the HFSP (AW) and the French Ministère de la Recherche et de l'Education (LR) for financial support, N. Gülüm and C. Nowak for expert technical assistance, W. Kabsch and F. Vellieux for advice, the staff at the EMBL c/o DESY synchrotron facility for support and B. Prakash for critical reading of the manuscript.

References

Aebi, M., Clark, M. W., Vijayraghavan, U. & Abelson, J. J. (1990). *Mol. Gen. Genet.* **224**, 72 80.

Bischoff, F. R. & Ponstingl, H. (1991). *Nature (London)*, **354**, 80–82.

Clark, K. L. & Sprague, G. F. Jr (1989). *Mol. Cell. Biol.* **9**, 2682–2694.

Collaborative Computational Project, Number 4 (1994). *Acta Cryst.* D**50**, 760–763.

Ducruix, A. & Giegé, R. (1992). *Crystallization of Nucleic Acids and Proteins: A Practical Approach*, pp. 99–126. Oxford: IRL Press.

Garboczi, D. N., Madden, D. R. & Wiley, D. C. (1994). *J. Mol. Biol.* **239**, 581–587.

Garman, E. F. & Schneider, T. R. (1997). *J. Appl. Cryst.* **30**, 211–237.

Kabsch, W. (1993). *J. Appl. Cryst.* **26**, 795–800.

Kadowaki, T., Goldfarb, D., Spitz, L. M., Tartakoff, A. M. & Ohno, M. (1993). *EMBO J.* **12**, 2929–2937.

Kai, R., Ohtsubo, M., Sekiguchi, M. & Nishimoto, T. (1986). *Mol. Cell Biol.* **6**, 2027–32.

Kirkpatrick, D. & Solomon, F. (1994). *Genetics*, **137**, 381–392.

Klebe, C., Bischoff, F. R., Ponstingl, H. & Wittinghofer, A. (1995). *Biochemistry*, **34**, 639–647.

Klebe, C., Nishimoto, T. & Wittinghofer, A. (1993). *Biochemistry*, **32**, 11923–11928.

Matsumoto, T. & Beach, D. (1991). *Cell*, **66**, 347–360.

Matthews, B. W. (1968). *J. Mol. Biol.* **33**, 491–497.

Meindl, A., Dry, K., Herrmann, K., Manson, F., Ciccodicola, A., Edgar, A., Carvalho, M. R., Achatz, H., Hellebrand, H., Lennon, A., Migliaccio, C., Porter, K., Zrenner, E., Bird, A., Jay, M., Lorenz, B., Wittwer, B., d'Urso, M., Meitinger, T. & Wright, A. (1996). *Nature Genet.* **13**, 35–42.

Nishitani, H., Ohtsubo, M., Yamashita, K., Iida, H., Pines, J., Yasudo, H., Shibata Y., Hunter, T. & Nishimoto, T. (1991). *EMBO J.* **10**, 1555–1564.

Otwinowski, Z. & Minor, W. (1993). *Data Collection and Processing. Proceedings of the CCP4 Study Weekend*, edited by L. Sawyer, N. Isaacs & S. Bailey, pp. 556–562. Warrington: Daresbury Laboratory.

Renault, L., Nassar, N., Vetter, I., Roth, M. & Wittinghofer, A. (1998). *Nature (London)*, **392**, 97–101.

Roepman, R., van Duijnhoven, G., Rosenberg, T., Pinckers, A. J., Bleeker-Wagemakers, L. M., Bergen, A. A., Post, J., Beck, A., Reinhardt, R., Ropers, H. H., Cremers, F. P. & Berger, W. (1996). *Hum. Mol. Genet.* **5**, 1035–1041.

Rosa, J. L., Casaroli-Marano, R. P., Buckler, A. J., Vilaró, S. & Barbacid, M. (1996). *EMBO J.* **15**, 4262–4273.

Rush, M. G., Drivas, G. & D'Eutachio, P. (1996). *BioEssays*, **18**, 103–112.

Sazer, S. & Nurse, P. (1994). *EMBO J.* **13**, 606–615.

Seino, H., Hisamoto, N., Uzawa, S., Sekiguchi, T. & Nishimoto, T. (1992). *J. Cell Sci.* **102**, 393–400.

Seki, T., Hayashi, N. & Nishimoto, T. J. (1996). *Biochemistry*, **120**, 207–214.

Uchida, S., Sekiguchi, T., Nishitani, H., Miyauchi, K., Ohtsubo, M. & Nishimoto, T. (1990). *Mol. Cell Biol.* **10**, 577–584.

Vellieux, F. M. D., Hunt, J. F., Roy, S. & Read, R. (1995). *J. Appl. Cryst.* **28**, 347–351.